Materials Science Forum *Online: 2004-08-15*
ISSN: 1662-9752, Vols. 461-464, pp 77-84
doi:10.4028/www.scientific.net/MSF.461-464.77

Yttrium Implantation and Addition Element Effects on the Oxidation Behaviour of Reference Steels at 973 K

E. Caudron, H. Buscail, R. Cueff, C. Issartel, S. El Messki, S. Perrier and F. Riffard

Laboratoire Vellave d'Elaboration et d'Etude des Matériaux, Univ. Blaise Pascal Clermont-Fd 2, B.P. 219, 43006 Le Puy en Velay, France. Email : Caudron@iut.u-clermont1.fr

Keywords : Steel, High temperature, Oxidation, Yttrium, Ion implantation.

Abstract. Yttrium implantation effects on reference steels (extra low carbon and low manganese steel) were studied by Rutherford Backscattering Spectrometry (RBS), Reflection High Energy Electron Diffraction (RHEED), X-ray Diffraction (XRD) and Glancing Angle X-ray Diffraction (GAXRD). Thermogravimetry and in situ X-Ray Diffraction at 700°C and P_{O2}=0.04 Pa for 24h were used to determine the yttrium implantation and addition element effects on sample oxidation resistance at high temperatures. This study clearly shows that yttrium implantation and subsequent high temperature oxidation induced the formation of several yttrium mixed oxides which closely depend on the reference steel addition elements. Moreover, these yttrium mixed oxides seem to be responsible for the improved reference steel oxidation resistance at high temperatures.

Introduction

Several studies demonstrate that ion implantation constitutes an interesting way to obtain a protective oxide scale improving metal or alloy corrosion resistances at high temperatures. In fact, ion implantation allows to incorporate a controlled concentration of oxygen reactive elements such as cerium, yttrium or hafnium into studied materials. Moreover, the incorporation of oxygen reactive elements (<1%) to the bulk alloy or to the surface allows to decrease the oxidation rate and to improve the scale adherence [1-9]. The aim of this study is to analyze the effects of yttrium implantation and addition elements on the high temperature oxidation resistance of various reference steels. This paper constitutes the next stage of our study concerning the effect of yttrium implantation on reference materials at high temperatures [10].

Experimental details

The compositions of the reference samples which are respectively extra low carbon steel (FeC) and low manganese steel (FeMn) are given in Table 1.

Table 1. ICPMS analyses of the reference steels investigated in this study (mass percentage).

Sample	C	Mn	P	S	Si	Al	Fe
Extra low carbon steel (FeC)	0.054	-	-	< 0.001	-	-	Bal
Low manganese steel (FeMn)	< 0.001	0.20	-	< 0.001	-	-	Bal

Rectangular specimens (surface area of around 3 cm^2 and 1 mm thick) are abraded up to 1200-grit SiC paper, polished up to 0.3 µm diamond paste, degreased with acetone and dried. This surface preparation is followed by yttrium implantation performed using a 180 keV energy beam corresponding to a nominal dose of 10^{17} ions/cm^2 by sample surface scanning using a 0.5 mm ion beam diameter for 106 minutes to obtain the entire surface implantation. Distributions of implanted yttrium were investigated by Rutherford backscattering spectrometry (RBS) using an alpha beam energy of 1.8 MeV (beam current : 10-50 nA range) [11, 12]. Reference steel structural evolutions (due to yttrium implantation) were investigated by reflected high energy electron diffraction (RHEED) (incident electron beam of 100 keV), classical X-ray diffraction (XRD) and glancing angle X-ray diffraction (GAXRD) using $CuK_{\alpha 1}$=1.540560 Å radiation. High temperature studies were performed for 24h at 700°C and P_{O2}=0.04 Pa using a Setaram TGDTA 92-1600 microthermobalance for mass gain and a high temperature Anton PAAR HTK 1200 chamber with integrated sample spinner in a Philips X'pert MPD diffractometer for X-ray diffraction studies. The experimental conditions (T=700°C ; P_{O2}=0.04 Pa) were chosen to avoid iron phase transformation (temperature) and to easily analyze the oxides grown during the oxidation test (pressure).

Results and discussion

Yttrium implanted and unimplanted sample oxidation kinetics at high temperature. Three unimplanted and yttrium implanted samples were used to check the reproducibility of specimen oxidation behaviour at high temperature. Fig. 1 shows the mean mass gain versus time curves of yttrium implanted and unimplanted reference steels oxidized for 24 h at 700°C under an oxygen partial pressure of 0.04 Pa. This figure clearly underlines two main results : firstly, the predominant role of addition elements on reference steel behaviour at high temperature and secondly, the benefit of implanting yttrium into the reference steels to increase their oxidation resistance at high temperature. Unimplanted low manganese steel exhibits the highest mass gain and follows a linear regime throughout the oxidation test with the corresponding linear rate constant $k_{1(FeMn)}$ = (2.9 ± 0.2).10^{-4} mg.cm^{-2}.s^{-1}. Unimplanted extra low carbon steel exhibits two linear parts : in the early phase of the oxidation test (during the first 10h) an important linear mass gain is observed corresponding to a linear rate constant $k_{1(FeC)}$ = (2.8 ± 0.2).10^{-4} mg.cm^{-2}.s^{-1} followed by a second low linear oxidation rate (after 10h) with a smaller mass gain corresponding to a linear rate constant : $k_{2(FeC)}$ = (0.44 ± 0.05).10^{-4} mg.cm^{-2}.s^{-1}. In fact, these results show that unimplanted low manganese steel exhibits the same high temperature linear oxidation rate as unimplanted pure iron [10]. These analyses clearly demonstrate that manganese alone has no influence on the oxidation rate in comparison with pure iron (under our experimental conditions). These results are confirmed by the oxide scale thickness (observed by SEM after 24h oxidation test) which is close to 250-270 µm and adherent to the substrate for both pure iron and low manganese steel. This phenomenon can be attributed to the low concentration of this element in the alloy and to the fast manganese diffusion into iron and iron oxides at high temperature as suggested by several authors [13, 14]. However, for unimplanted low manganese steel, thin deposits were observed inside the quartz tubes used for thermogravimetric analyses, suggesting the evaporation of volatile compounds condensed on the cold parts of these quartz tubes. X-ray analyses performed on low manganese condensed deposits indicate that these deposits correspond to the same compound i.e. Mn_3O_4 (JCPDS 24-734), which is in good agreement with thermodynamic data showing that Mn_3O_4 is a volatile oxide under our experimental conditions [15, 16]. Thermogravimetric results obtained on unimplanted extra low carbon steel clearly demonstrate that carbon has a major effect on the oxidation rate as suggested by the resulting low mass gain and oxide scale thickness (observed by SEM) which is 100 µm. The presence of this element could be responsible for the formation of iron carbides or $(Fe,Mn)_3C$ which have good stability at high temperatures but which contribute to a lower adherence of the oxide scales as observed by several authors [17, 18]. The Wagner model and other theories based on iron self-diffusion acting as an iron oxidation limiting step [19-21] imply a parabolic oxidation regime. The oxidation behaviour of unimplanted low manganese steel rather suggests that the scale growth is limited by the adsorption rate of O_2 molecules on the oxide scale surface as previously suggested for pure iron [10]. The particular behaviour of unimplanted extra low carbon steel mass gain curve suggests the combination of two phenomena : a scale growth limited by O_2 molecules adsorption rate on the oxide scale surface (as in the case of low manganese steel) and the formation of carbides (carbon enrichments were detected by energy dispersive X-ray spectrometry (EDXS) at the metal-oxide interface), promoting important localized oxide scale detachments from the substrate, which seem to be responsible for the variation in the linear oxidation rate as observed in Fig. 1.

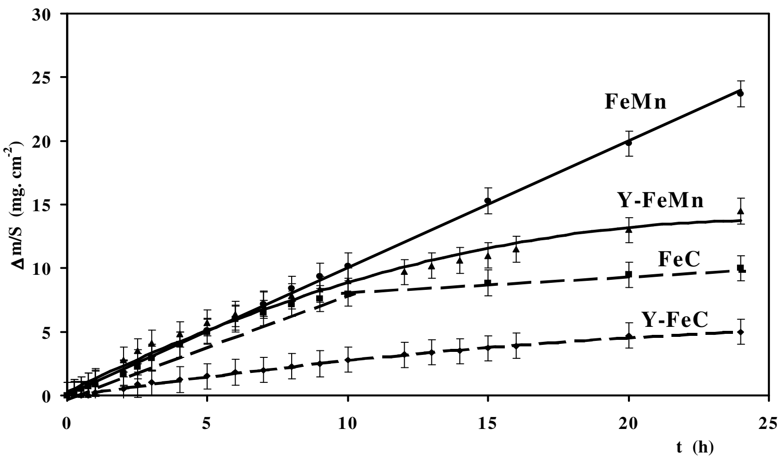

Fig. 1. Mean mass gain vs. time curves of yttrium implanted and unimplanted steels (T=700°C ; P_{O2} = 0.04 Pa).

The oxidation behaviour of both yttrium implanted extra low carbon steel and low manganese steel clearly shows that yttrium implantation leads to parabolic oxidation instead of linear oxidation as observed in the case of unimplanted samples. Yttrium implanted extra low carbon steel mass gain data show that, in the early phase of oxidation, a latent period of about 45 minutes is observed during which there is no mass gain, followed by a parabolic regime ($k_{p(YFeC)}$ = (0.51 ± 0.04) $.10^{-3}$ $mg^2.cm^{-4}.s^{-1}$). Yttrium implanted low manganese steel mass gain curve exhibits a latent period of about 30 minutes in the early stage of the oxidation test during which no mass gain is detected followed by a parabolic regime ($k_{p(YFeMn)}$ = (3.1 ± 0.3) $.10^{-3}$ $mg^2.cm^{-4}.s^{-1}$). The parabolic rates observed in the case of yttrium implanted steels rather suggest that iron self-diffusion is the iron oxidation limiting step whatever the yttrium implanted sample as suggested by the Wagner model. Moreover, the oxide scales present a better adherence than those of unimplanted samples and their thicknesses (measured by SEM) after the 24 h oxidation test are respectively 30 µm (extra low carbon steel) and 100 µm (low manganese steel) which confirms that yttrium implantation increases the oxidation resistance of the reference steels at high temperature. These results have prompted us to carry out in situ high temperature X-ray diffraction studies in order to understand the different mass gain curve evolutions obtained by thermogravimetry in the case of unimplanted and yttrium implanted reference steels.

In situ high temperature X-ray diffraction characterization of unimplanted steels. In situ high temperature X-ray analyses (T = 700°C ; P_{O2} = 0.04 Pa) were performed every 30 minutes for 24 hours on both yttrium implanted and unimplanted steels. Initial sample and the 24-h in situ oxidation test X-ray analyses of extra low carbon steel (Fig. 2) and low manganese steel (Fig. 3) allow us to observe the initial growth stage of the well-known triple iron-oxide layer (FeO (at the greatest depths) / Fe_3O_4 (at intermediate depths) / Fe_2O_3 (near the oxide-gas interface)) according to the sample nature. These figures show that Fe characteristic diffraction peaks (JCPDS 6-696) with the (110) preferential orientation have completely disappeared during the first 30-min. oxidation test whatever the sample nature. Comparison of the evolution of the characteristic diffraction peaks of

FeO (wustite : JCPDS 6-615), Fe_3O_4 (magnetite : JCDPS 19-629) and Fe_2O_3 (hematite : JCPDS 33-664) reveals that the growth of these three iron oxides closely depends on the addition elements.

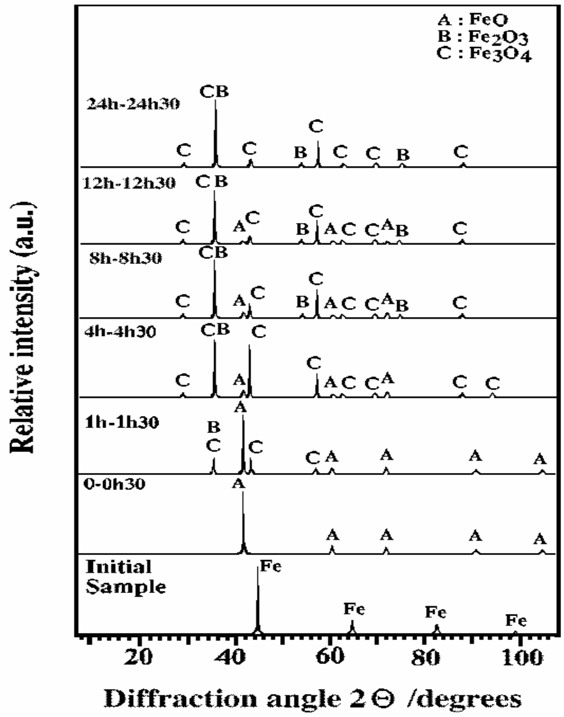

Fig. 2. In situ high temperature 24h30 XRD main experimental diffractograms performed on unimplanted extra low carbon steel (T=700°C ; P_{O2} = 0.04 Pa).

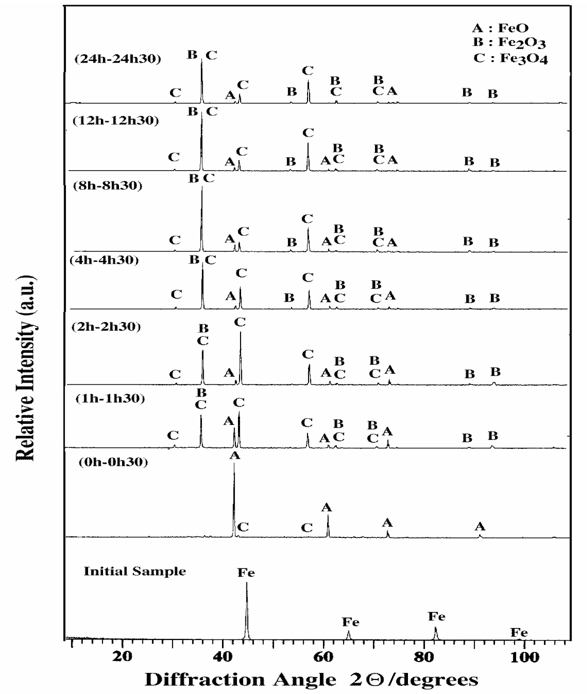

Fig. 3. In situ high temperature 24h30 XRD main experimental diffractograms performed on unimplanted low manganese steel (T=700°C ; P_{O2} = 0.04 Pa).

In the case of extra low carbon steel (Fig. 2), only the initial growth of FeO is detected during the first 30-min. oxidation test with the (200) main characteristic peak (2θ = 41.93°) independent of the substrate (110) orientation. After the first hour, Fe_3O_4 and small amounts of Fe_2O_3 were also detected. However, the peak near 2θ = 35.5° corresponds in fact to the overlapping of characteristic diffraction peaks of Fe_3O_4(311) at 2θ = 35.4° (relative intensity : 100%) and Fe_2O_3(110) at 2θ = 35.6° (relative intensity : 70%). The evolution of the main characteristic diffraction peaks of iron oxides clearly shows that during the first 4h of the oxidation test the Fe_3O_4 layer presents an initial nucleation stage with the (400) preferential orientation (2θ = 43.05°) imposed by the FeO sublayer (200) orientation. After this period, the Fe_3O_4 layer regains its (311) normal orientation (magnetite major peak only resulting from the structure factor contribution). After 12h of the oxidation test, the FeO characteristic diffraction peaks become undetectable, which clearly demonstrates the presence of this compound in the depths of the extra low carbon steel. The Fe_2O_3 low characteristic intensity peaks indicate the presence of this compound in the form of a thin layer at the gas-oxide interface. However, no iron carbides were identified by XRD, which can be explained by concentrations of the iron carbide nanocrystalline phases below the detection limit of our XRD equipment. By contrast, in the case of low manganese steel (Fig. 3) FeO(200) and Fe_3O_4(400) characteristic diffraction peaks are directly detected during the first stages of the oxidation test. Interestingly enough, the characteristic diffraction peak intensities of these compounds are higher than those observed for extra low carbon steel, which is in good agreement with the results obtained by thermogravimetry (low manganese steel highest mass gain). Similar evolutions are observed concerning the triple iron-oxide layer formation but FeO characteristic diffraction peaks are observable throughout the oxidation test as in the case of pure iron [10] which confirms the minor role of manganese on the oxidation rate of iron as suggested by thermogravimetric results.

Yttrium implantation effect on reference steels before oxidation test. RBS analyses indicate the presence of oxygen in all yttrium implanted samples which can be explained by the combination of two phenomena : the sputtering of the naturally oxidized sample surfaces during the implantation process and the low oxygen partial pressure (lower than 10^{-2} Pa) existing in the implantation chamber. RBS results also show that yttrium penetrates as deep as about 110-120 nm and the yttrium maximum concentration is near a 35-40 nm depth whatever the sample nature. Oxygen and yttrium distribution evolutions suggest the formation of several oxides depending on the yttrium implantation depth. For the lowest yttrium implantation depths (down to 35 nm), RBS analyses give O/Y ratios varying from 6 to 1.5. The most interesting result lies in that the O/Y ratios obtained near the 35 nm depth are slightly greater than 1.5 whatever the reference steel tested in our study. This result seems to suggest the presence of the same yttrium oxide (Y_2O_3). Indeed, some authors [22-24] have pointed out that Y_2O_3 promotes the corrosion resistance of Cr_2O_3 and Al_2O_3 subsequent protective coatings against corrosive environments. XRD analyses of extra low carbon (Fig. 7) and low manganese steels (Fig. 8) clearly show the presence of Y_2O_3 (JCPDS 41-1105) in addition to the α-Fe substrate structure (JCPDS 06-696) as suggested by RBS. However, this first batch of structural analyses is not sufficient to draw conclusions on the yttrium implantation effect because classical XRD analysis is not a very sensitive technique for the determination of very low nanocrystalline phase. Hence, RHEED and GAXRD techniques, which are more sensitive surface techniques than classical XRD, have been used to confirm the validity of these previous results.

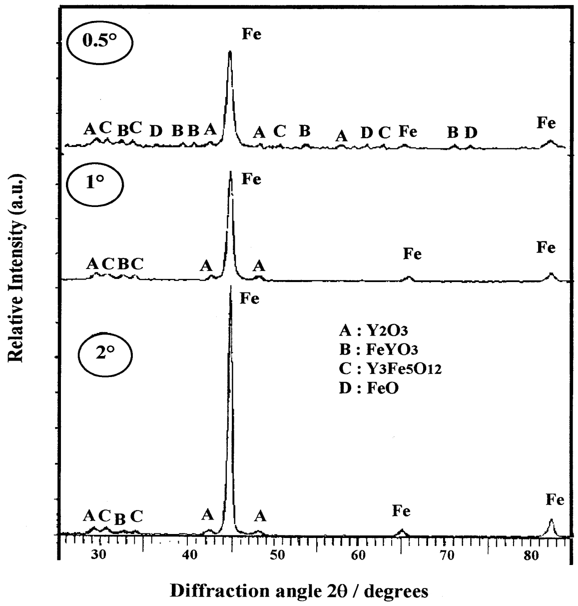

Fig. 4. GAXRD experimental diffractograms for yttrium implanted extra low carbon steel performed at various glancing incidences.

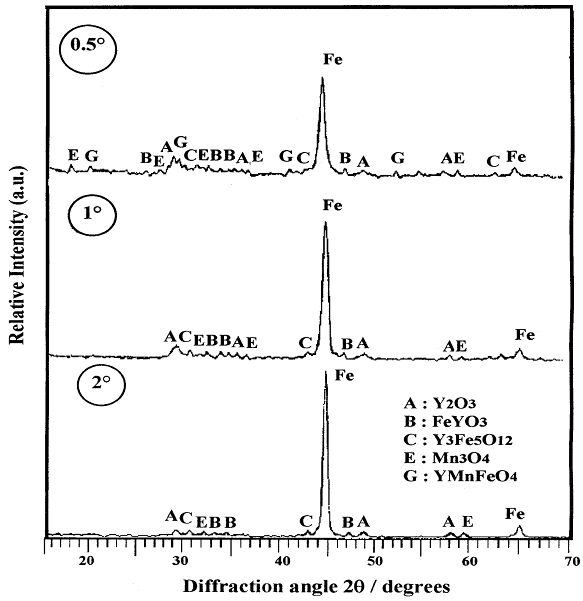

Fig. 5. GAXRD experimental diffractograms for yttrium implanted low manganese steel performed at various glancing incidences.

RHEED analyses of extra low carbon steel identified the alpha iron structure (JCPDS 06-696) and the FeO wustite (JCPDS (06-615)) compound whereas RHEED analyses performed on the low manganese steel showed only the characteristic diffraction values corresponding to the α-Fe structure. However, some amorphous compounds, undetectable by structural techniques, may also be present in the implanted depth, which could explain the high O/Y and O/Fe ratios observed near the surface by RBS. To complete the structural analyses, GAXRD investigations were carried out on each specimen using glancing angles ranging from 0.5° to 2° which correspond to maximum theoretical penetration depths of approximately 40 nm to 180 nm, depending on the incident angle and the nature of the sample. This glancing angle range was chosen in order to observe the initial growths of any possible nanocrystalline oxide phases close to the surface. GAXRD diffractograms of the extra low carbon steel (Fig. 4) show the presence of Y_2O_3 (41-1105) and FeO (6-615) as previously found by XRD and RHEED techniques. Fig. 4 shows that other yttrium-iron mixed oxides, such as $Y_3Fe_5O_{12}$ (JCPDS 43-507) and $FeYO_3$ (JCPDS 39-1489), also seem to be formed after yttrium implantation. However, GAXRD analyses show that Y_2O_3, $Y_3Fe_5O_{12}$ and $FeYO_3$ are present whatever the implantation depth whereas FeO compound only occurs near the surface. GAXRD analyses performed on the low manganese steel (Fig. 5) also show the presence of the Y_2O_3, $Y_3Fe_5O_{12}$ and $FeYO_3$ compounds. It can be noted that two other compounds seem to be formed during yttrium implantation, these are $YMnFeO_4$ (JCPDS 36-961) and Mn_3O_4 (JCPDS 24-734). However, GAXRD analyses suggest that $YMnFeO_4$ occurs mainly close to the surface. All the GAXRD diffractograms show decreases in the typical iron peak relative intensity, irrespective of the nature of the sample, which confirms the formation of several new compounds in the implanted depth. The most interesting result lies in the fact that GAXRD analyses tend to prove that three compounds (i.e. Y_2O_3, $Y_3Fe_5O_{12}$ and $FeYO_3$) are always formed during yttrium implantation whatever the reference steel which clearly shows the higher affinity for oxygen of yttrium compared to that of iron. It is important to note that in the case of low manganese steel, GAXRD analyses reveal the presence of manganese and yttrium-manganese-iron oxides which are very difficult to identify by RHEED because of a possible overlapping of characteristic peaks that are not easy to distinguish by RHEED. The presence of Mn_3O_4 and $YMnFeO_4$ also underlines the higher oxygen affinity of manganese compared to that of iron. The combined results of all structural techniques (XRD, RHEED and GAXRD) are in good agreement with those obtained by RBS.

In situ high temperature X-ray analyses of yttrium implanted reference steels. Initial yttrium implanted extra low carbon steel and the most interesting in situ X-ray diffractograms obtained during the 24h oxidation test are given in Fig. 6. This figure suggests an important yttrium diffusion out of extra low carbon steel because Y_2O_3 oxide promoted by yttrium implantation has completely disappeared after the first 30 min. of the oxidation test. The most interesting result is the fact that the main iron (110) characteristic diffraction peak is still observable after 1h of the oxidation test whereas no iron peak was observable after the first 30 min. oxidation test for unimplanted sample. These results are in good agreement with the 45 min. latent period observed by thermogravimetry during which no mass gain was detected for implanted sample. Figure 6 also shows that two main compounds (i.e. $FeYO_3$ (121) (JCPDS 39-1489) and Fe_2YO_4 (300) (JCPDS 32-477)) seem to be promoted along with the FeO (200), Fe_3O_4 ((400) at the beginning and (311) at the end of the oxidation test) and Fe_2O_3 (110) structures by the oxidation test. It is interesting to note that FeO(200), Fe_2YO_4(300), Fe_3O_4(400) compounds exhibit similar preferential orientations. By contrast, the $FeYO_3$(121) main characteristic diffraction peak suggests that the initial nucleation stage of this compound is independent of the FeO, Fe_3O_4 and Fe_2YO_4 preferential orientations. Moreover, the presence of yttrium-mixed oxides seems to limit the magnetite growth as suggested by the fact that Fe_3O_4 regains more slowly its (311) typical orientation. The formation of the two yttrium-iron oxides (i.e. $FeYO_3$ and Fe_2YO_4), observed by in situ X-ray diffraction, can be attributed to the high oxygen reactivity of yttrium which may promote the transformation of the Y_2O_3 and Fe_2O_3 phases into $FeYO_3$ and the transformation of Fe_3O_4 spinel-type structure into Fe_2YO_4. Fe_2YO_4 structure growth may be also attributed to the combination of $FeYO_3$ and FeO compounds. Moreover, the transformation of the $Y_3Fe_5O_{12}$ phase, induced by yttrium implantation, could also lead to the formations of $FeYO_3$ and Fe_2YO_4 phases. The evolution of $FeYO_3$ and Fe_2YO_4 characteristic peaks during the 24 h oxidation test seems to suggest that these compounds are mainly located at the gas-oxide interface. These yttrium-iron mixed oxides seem to limit the growth of the iron oxides (lower diffraction peak intensities than those observed for unimplanted samples).

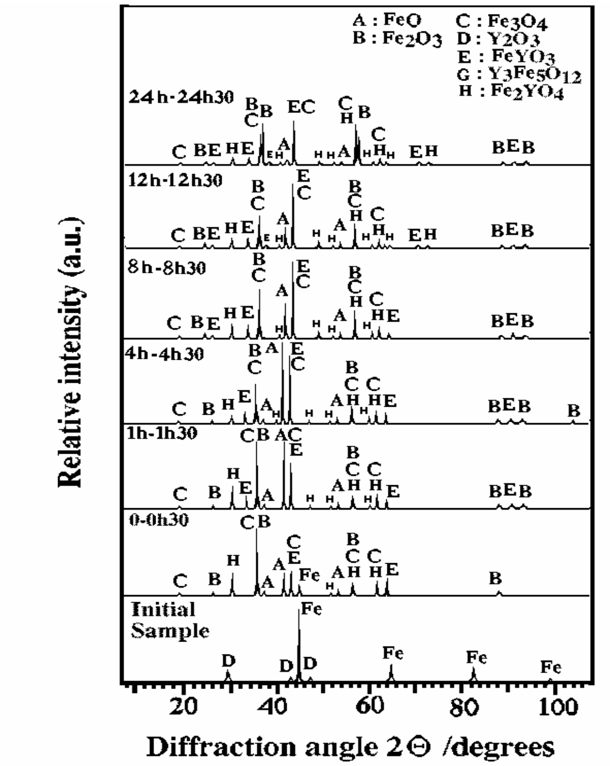

Fig. 6. In situ high temperature 24h30 XRD main diffractograms performed on yttrium implanted extra low carbon steel (T=700°C ; P_{O2} = 0.04 Pa).

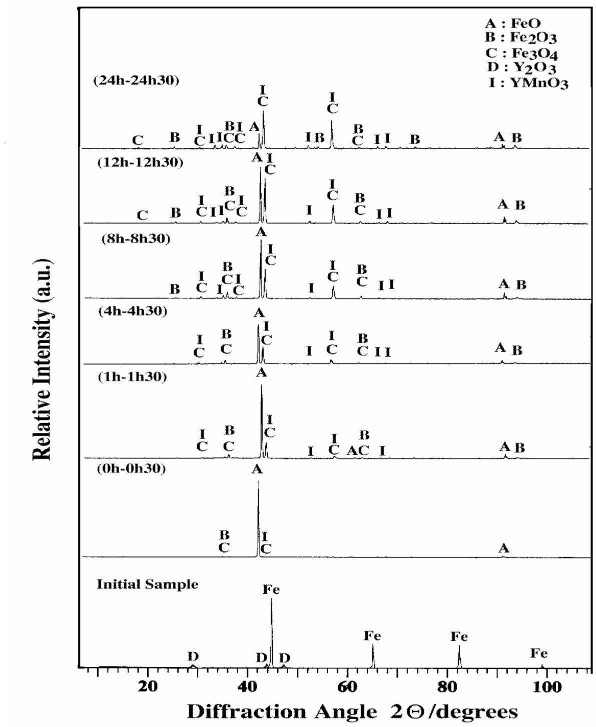

Fig. 7. In situ high temperature 24h30 XRD main diffractograms performed on yttrium implanted low manganese steel (T=700°C ; P_{O2} = 0.04 Pa).

XRD main experimental diffractograms for the initial yttrium implanted low manganese steel (before oxidation) and the 24 h in situ high temperature oxidation test are given in Fig. 7. This figure shows that one compound, i.e. $YMnO_3$ (JCPDS 25-1079) with the (114) preferential orientation, seems to be promoted along with the wustite, hematite and magnetite structures. The evolution of $YMnO_3$ characteristic diffraction peaks seems to suggest that this compound is mainly localized at the oxide-gas interface with a preferential orientation independent of those of iron oxides. Interestingly enough, X-ray diffraction analyses also show that yttrium implantation substantially limits the growth of the FeO and Fe_3O_4 layers compared to unimplanted sample (Fig. 3), as suggested by the corresponding mass gain curves (Fig. 1). In fact, in situ X-ray analyses show that the main Fe_3O_4 diffraction peak is still the (400) peak, imposed by the FeO (200) sublayer, throughout the 24h oxidation test which clearly demonstrates that $YMnO_3$ formation limits substantially the growth of the Fe_3O_4 layer which could not regain its normal (311) orientation. The formation of the yttrium-manganese oxide in low manganese steel instead of yttrium-iron mixed oxides (as observed for extra low carbon steel) can be attributed to several mechanisms. Firstly, yttrium and manganese have higher oxygen affinity compared to that of iron which could lead to the formation of $YMnO_3$ instead of $YFeO_3$. Secondly, the high manganese diffusion into iron and iron-oxides at high temperature [13, 15] could lead to the dissociation of the $YMnFeO_4$ compound (observed after yttrium implantation) into $YMnO_3$ and FeO, and to the formation of $YMnO_3$ by the combination of Y_2O_3 (observed after yttrium implantation) and Mn_2O_3 (induced by high temperature oxidation test). Moreover, no deposits were observed on the cold parts of the quartz tubes used for thermogravimetric analyses, which clearly indicates that $YMnO_3$ growth substantially limits the Mn_3O_4 evaporation observed in the case of unimplanted samples. The $YMnO_3$ layer in low manganese steel, acting as an iron diffusion barrier layer, substantially limits the formation of iron-oxides in the sample which is confirmed by the low parabolic rate observed by thermogravimetry.

Conclusion

This work shows the successful contribution of in situ high temperature X-ray diffraction to the understanding of the initial growth stage of the triple iron-oxide layer ($FeO/Fe_3O_4/Fe_2O_3$) according to the reference steel addition element. Structural analyses obtained by XRD, RHEED and GAXRD are in good agreement with RBS results because these techniques make it possible to identify the main oxides formed during yttrium implantation according to the steel addition elements. The most interesting result is that in situ high temperature X-ray diffraction clearly demonstrates that yttrium implantation induces, during the oxidation at high temperature, the formation of protective yttrium-iron mixed oxides at the oxide-gas interface which closely depend on reference steel addition elements. These results emphasize that yttrium implantation offers a new possibility of increasing the oxidation resistance of various steels at high temperature by controlling the effects of addition elements.

References

[1] I.M. Allam, D.P. Whittle and J. Stringer: Oxid. Met. Vol. 12 (1978), p. 35
[2] J. Stringer: Mat. Sci. Eng. Vol. A120 (1989), p. 129
[3] F.I. Wei and F.H. Stott: Corros. Sci. Vol. 29 (1989), p.839
[4] D.P. Moon and M.J. Bennett: Mat. Sci. Forum Vol. 43 (1989), p. 269
[5] J. Jedlinski: Corros. Sci. Vol. 35 (1993), p. 863
[6] B. Pieraggi and R.A. Rapp, J. Phys. IV Vol. 9 (1993), p.275
[7] B.A. Pint, A.J. Garratt-Reed and L.W. Hobbs: J. Phys. IV Vol. 9 (1993), p. 247
[8] H. Buscail, C. Courty, and J.P. Larpin: J. Phys. IV vol. 5 (1995), p. 375
[9] H. Buscail, J.P. Larpin, E. Caudron, R. Cueff, F. Riffard, F. Rabaste and M.F. Stroosnijder: Mater. Sci. Forum Vol. 369-372 (2001), p. 483
[10] E. Caudron, H. Buscail, R. Cueff, V.Haanapel, Y.P. Jacob, F. Riffard and M.F. Stroosnijder: Mater. Sci. Forum Vol. 369-372 (2001), p. 817
[11] E. Caudron, H. Buscail, Y.P. Jacob, C. Courty and M.F. Stroosnijder: Solid State Ionics Vol. 112 (1998), p. 361
[12] E. Caudron, H. Buscail, Y.P. Jacob, C. Josse-Courty, F. Rabaste and M.F. Stroosnijder: Nucl. Instr. Meth. Vol. B155 (1999), p. 91
[13] Y. Ueshima, H. Schmalzried and J. Koepke: J., Phil. Mag. Vol. A61 (1990), p. 707
[14] Y. Ueshima and H. Schmalzried: Phil. Mag. Vol. A61 (1990), p. 725
[15] J.B. Price and J.B. Wagner: J. Electrochem. Soc. Vol. 117 (1970), p. 242
[16] D.L. Douglass and F. Rizzo-Assuncao: Oxid. Met. Vol. 29 (1998), p. 271
[17] J. Manenc and G. Vagnard: Corros. Sci. Vol. 9 (1969), p. 857
[18] U. Malik and D.P. Whittle: Oxid. Met. Vol. 16 (1981), p. 339
[19] C. Wagner: *Atomic Movements* (American Society of Metallurgy, Cleveland 1951).
[20] P. Kofstad: *High Temperature Corrosion* (Elsevier Applied Science, London 1988).
[21] G. Hettich, H. Mehrer and K. Maier: Scripta Metall. Vol. 11 (1977), p. 795
[22] K. Przbylski and G.J. Yurek: Mater. Sci. Forum Vol. 43 (1989), p. 1
[23] A. Strawbridge and P.Y. Hou: J. Mater. High Temp. Vol. 12 (1994), p. 177
[24] S. Seal, S.K. Bose and S.K. Roy: Oxid. Met. Vol. 41 (1994) p. 139